Chapter 1

Conduction Electrons and Fermi Surfaces

Conduction electrons are described by the one-electron band theory in which the electron-electron interactions (correlations) are simply neglected at the start. The Schrödinger wave function is solved for an electron moving in a potential which varies periodically with distance. The corresponding Bloch state with a band width of a few eV develops in the whole crystal. The conduction electrons are thus well described in momentum (k) space. The conduction electrons have energies up to a Fermi energy $\varepsilon_{\rm F}$, which is simply expressed by $\varepsilon_{\rm F} = \frac{1}{2}mv_{\rm F}^2 = (\hbar k_{\rm F})^2/2m$. The Fermi surface is thus defined as a constant energy surface in k space of which the energy is equal to $\varepsilon_{\rm F}$. Even though the electron-electron interactions may change the topology of the Fermi surface, the volume of the Fermi surface is kept invariant. It is the boundary of the electronic momentum distribution in the ground state, dividing k space sharply into two regions which electrons occupy or do not occupy. Note that the mass of the correlated conduction electron is changed from the bare mass m or the band mass $m_{\rm b}$ to an effective mass m^*.

1.1 Non-interacting conduction electrons -Fermi gas-

Strong magnetism described in the present text is present in the compounds containing the first-line series of transition metals (Ti, V, Cr,

Mn, Fe, Co, Ni, Cu), lanthanoids (lanthanides) (Ce, Pr, Nd, Sm, Eu, Gd, Tb, Dy, Ho, Er, Tm, Yb), and actinoids (actinides) (U, Np, Pu, Am, Cm). Their electron configurations are as follows

transition metals [Ar core] $3d^n\boldsymbol{4s^2}$ $(n = 0 - 10)$

lanthanides [Kr core] $4f^n5s^25p^6\boldsymbol{5d^16s^2}$ $(n = 0 - 14)$

actinides [Xe core] $5f^n6s^26p^6\boldsymbol{6d^17s^2}$ $(n = 0 - 14)$.

Three series of elements play a fundamental role in magnetism because $3d$, $4f$, and $5f$ shells can remain unfilled, leading to magnetism in the crystal. Note that $4d$, $5d$, and $6d$ electrons are rather delocalized, participating in the conduction band, and their contribution to magnetism is generally very weak. The $4s^2$ electrons in transition metals, $5d^16s^2$ electrons in lanthanides, and $6d^17s^2$ electrons in actinides contribute to the energy band, and partially become the conduction electrons.

First, we consider the conduction electrons based on a free electron model; that is, we consider N number of conduction electrons in a cubic crystal of length L, as shown in Fig. 1.1(a). The Schrödinger wave equation is

$$\left[-\frac{\hbar^2}{2m}\nabla^2 + V(\boldsymbol{r})\right]\Psi(\boldsymbol{r}) = \varepsilon\Psi(\boldsymbol{r}), \tag{1.1}$$

where the conduction electrons move freely in the crystal, as in an ideal gas. The one-particle wave function Ψ is expressed as Eq. (1.1), where the position $\boldsymbol{r} = (x, y, z)$, the wave vector $\boldsymbol{k} = (k_x, k_y, k_z)$, the potential energy $V(\boldsymbol{r})$, and

$$\nabla^2 = \frac{\partial^2}{\partial x^2} + \frac{\partial^2}{\partial y^2} + \frac{\partial^2}{\partial z^2}.$$

If we assume $V(\boldsymbol{r}) = 0$,

$$\Psi(\boldsymbol{r}) = \frac{1}{L^{3/2}}e^{i\boldsymbol{k}\cdot\boldsymbol{r}} \tag{1.2}$$

$$\varepsilon = \frac{\hbar^2\boldsymbol{k}^2}{2m} = \frac{\hbar^2}{2m}\left(k_x^2 + k_y^2 + k_z^2\right) \tag{1.3}$$

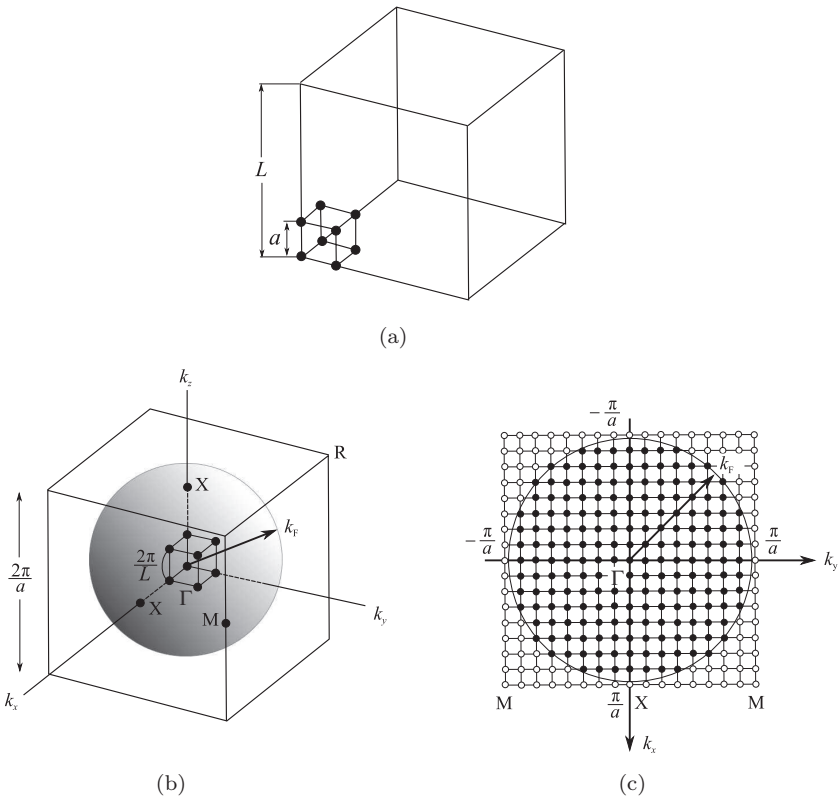

Figure 1.1: (a) Cubic crystal with a length L and the lattice constant a, (b) the corresponding spherical Fermi surface, and (c) the cross-section of the Fermi surface.

The wave function is conveniently required to be periodic in x, y, z with the length L, so that

$$\Psi(x, y, z + L) = \Psi(x, y, z), \quad \Psi(x, y + L, z) = \Psi(x, y, z),$$
$$\Psi(x + L, y, z) = \Psi(x, y, z), \tag{1.4}$$

which is called a periodic boundary condition. The wave vectors in x, y, z become

$$k_x = \frac{2\pi}{L} n_x, \quad k_y = \frac{2\pi}{L} n_y, \quad k_z = \frac{2\pi}{L} n_z$$
$$n_x,\ n_y,\ n_z = 0,\ \pm 1,\ \pm 2,\ \cdots .$$

The conduction electrons with number N occupy the energy states in momentum k-space, as shown in Fig. 1.1(b). Note that one energy state corresponds to a volume of $(2\pi/L)^3$ in k-space and is occupied by two electrons with the up and down spin states ($\uparrow$, $\downarrow$). The number of energy states Ω and the density of states $D(\varepsilon)$ in a Fermi sphere of radius k are expressed as

$$\Omega = \frac{\frac{4}{3}\pi k^3}{\left(\frac{2\pi}{L}\right)^3} = \frac{V}{6\pi^2}\left(\frac{2m\varepsilon}{\hbar^2}\right)^{3/2} \tag{1.5}$$

$$D(\varepsilon) = \frac{d\Omega}{d\varepsilon} = \frac{V}{4\pi^2}\left(\frac{2m}{\hbar^2}\right)^{3/2}\varepsilon^{1/2} \tag{1.6}$$

where

$$V = L^3, \quad \varepsilon = \frac{\hbar^2 k^2}{2m}.$$

The electronic specific heat coefficient γ, which is obtained experimentally by measuring the specific heat C, is related to the density of states $D(\varepsilon_{\rm F})$ at the Fermi energy $\varepsilon_{\rm F}$ as

$$\gamma = \frac{2\pi^2}{3}k_{\rm B}^2 D(\varepsilon_{\rm F}). \tag{1.7}$$

Note that $\gamma = (\pi^2/3)k_{\rm B}^2 D(\varepsilon_{\rm F})$ is often written in the text. In such a case, the density of states $D(\varepsilon_{\rm F})$ contains a factor of 2 based on the up and down spin states. The present density of states in Eq. (1.6) does not contain the factor of 2.

We now consider N conduction electrons in the cube $V(= L^3)$. The number of conduction electrons per unit volume, n, is given as

$$\begin{aligned} n = \frac{N}{V} &= \frac{1}{V}\int_0^{\varepsilon_{\rm F}} 2D(\varepsilon)d\varepsilon \\ &= \int_0^{\varepsilon_{\rm F}} \frac{1}{2\pi^2}\left(\frac{2m}{\hbar^2}\right)^{3/2}\varepsilon^{1/2}d\varepsilon \\ &= \frac{1}{3\pi^2}\left(\frac{2m}{\hbar^2}\right)^{3/2}\varepsilon_{\rm F}^{3/2} \end{aligned} \tag{1.8a}$$

or

$$\varepsilon_{\rm F} = \frac{\hbar^2}{2m}(3\pi^2 n)^{2/3}. \tag{1.8b}$$

Here, we consider the simple cubic structure with a lattice constant $a(=4\,\text{Å})$, and assume one atom possesses one conduction electron, which is confined in the crystal of the cube of length $L(=1\,\text{cm})$. The carrier number $n(=1/a^3)$ is $1.6\times10^{22}\,\text{cm}^{-3}$, which leads to $\varepsilon_\text{F}=2.3\,\text{eV}$ from Eq. (1.8b), or the Fermi temperature $T_\text{F}(=\varepsilon_\text{F}/k_\text{B})=27000\,\text{K}$, and the Fermi velocity $v_\text{F}(=\hbar k_\text{F}/m=\sqrt{2\varepsilon_\text{F}/m})=9.0\times10^7$ cm/s, where m is assumed to be m_0 (the electron rest mass).

Next, we consider the Schrödinger wave equation in Eq. (1.1) when the potential $V(\boldsymbol{r})$ exists but is weak. Both the wave function Ψ and potential V are periodic over a and therefore are expressed by Fourier expansions as

$$\Psi(\boldsymbol{r})=e^{i\boldsymbol{k}\cdot\boldsymbol{r}}u(\boldsymbol{r})=e^{i\boldsymbol{k}\cdot\boldsymbol{r}}\sum_{n'}u_{n'}e^{-i\boldsymbol{G}_{n'}\cdot\boldsymbol{r}} \tag{1.9}$$

$$V(\boldsymbol{r})=\sum_m V_m e^{-i\boldsymbol{G}_m\cdot\boldsymbol{r}} \tag{1.10}$$

where $\boldsymbol{G}_m$ is the reciprocal lattice vector. From Eqs. (1.1), (1.9) and (1.10), we can obtain the wave function Ψ and the eigenvalue ε as

$$\Psi(\boldsymbol{r})=u_0e^{i\boldsymbol{k}\cdot\boldsymbol{r}}+\sum_{n\neq0}\frac{V_n}{\frac{\hbar^2\boldsymbol{k}^2}{2m}-\frac{\hbar^2}{2m}(\boldsymbol{k}-\boldsymbol{G}_n)^2}u_0e^{i(\boldsymbol{k}-\boldsymbol{G}_n)\cdot\boldsymbol{r}} \tag{1.11}$$

$$\varepsilon=\frac{\hbar^2\boldsymbol{k}^2}{2m}+V_0+\sum_{n\neq0}\frac{|V_n|^2}{\frac{\hbar^2\boldsymbol{k}^2}{2m}-\frac{\hbar^2}{2m}(\boldsymbol{k}-\boldsymbol{G}_n)^2} \tag{1.12}$$

where $V_{-n}V_n=|V_n|^2$.

When $\hbar^2\boldsymbol{k}^2/2m=(\hbar^2/2m)(\boldsymbol{k}-\boldsymbol{G}_n)^2$ in Eq. (1.12),

$$\varepsilon=V_0+\frac{1}{2}\left\{\frac{\hbar^2\boldsymbol{k}^2}{2m}+\frac{\hbar^2}{2m}(\boldsymbol{k}-\boldsymbol{G_n})^2\right\}$$
$$\pm\sqrt{\left\{\frac{1}{2}\left[\frac{\hbar^2\boldsymbol{k}^2}{2m^*}+\frac{\hbar^2}{2m^*}(\boldsymbol{k}-\boldsymbol{G_n})^2\right]\right\}^2+|V_n|^2}. \tag{1.13a}$$

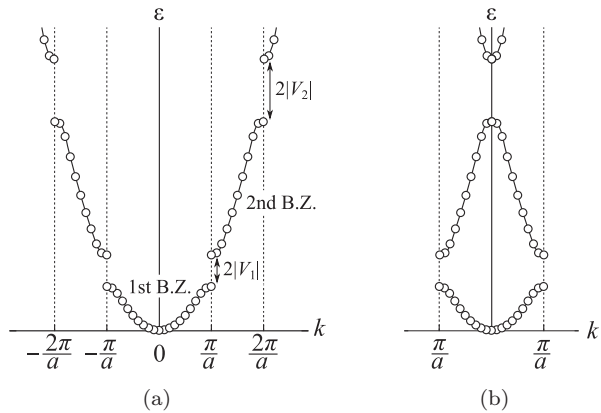

Figure 1.2: (a) Simplified energy band structure and (b) the corresponding one in the reduced zone scheme.

If we simplify the expansion by setting $G_n = (2\pi/a)n$ or $k = (\pi/a)n$,

$$\varepsilon = V_0 + \frac{\hbar^2}{2m}\left(\frac{\pi}{a}n\right)^2 \pm |V_n|. \tag{1.13b}$$

Figure 1.2(a) shows the simple energy band structure, where the energy band in the region of $k = -\pi/a$ to π/a is called the first Brillouin zone, while that in the region of $k = -2\pi/a$ to $-\pi/a$ and π/a to $2\pi/a$ is the second Brillouin zone. The energy gap at $k = (\pi/a)n$ is $2|V_n|$, which is expressed by the Fourier expansion coefficient V_n of the potential $V(\boldsymbol{r})$. The usual band structure is expressed in the reduced zone scheme, as shown in Fig. 1.2(b).

Note that the energy gap or the band gap is produced by the periodicity of the potential, which is called the Bragg reflection. The condition of the Bragg reflection, $\hbar^2\boldsymbol{k}^2/2m = (\hbar^2/2m)(\boldsymbol{k}-\boldsymbol{G}_n)^2$, is expressed as

$$\frac{|\boldsymbol{G}_n|}{2} = \boldsymbol{k}\cdot\frac{\boldsymbol{G}_n}{|\boldsymbol{G}_n|}. \tag{1.14}$$

This means that the zone boundary is normal to $\boldsymbol{G}_n$ at its midpoint. For example, the primitive lattice vector in the simple cubic crystal, as shown in Fig. 1.1(a), is

$$\boldsymbol{a}_1 = a\boldsymbol{i}, \quad \boldsymbol{a}_2 = a\boldsymbol{j}, \quad \boldsymbol{a}_3 = a\boldsymbol{k}$$

where $\boldsymbol{i}$, $\boldsymbol{j}$, and $\boldsymbol{k}$ are orthogonal unit vectors. The reciprocal lattice vector $\boldsymbol{b}_i$ is defined as $\boldsymbol{a}_i \cdot \boldsymbol{b}_j = 2\pi\delta_{ij}$, which leads to

$$\boldsymbol{b}_1 = \frac{2\pi}{a}\boldsymbol{i}, \quad \boldsymbol{b}_2 = \frac{2\pi}{a}\boldsymbol{j}, \quad \boldsymbol{b}_3 = \frac{2\pi}{a}\boldsymbol{k}.$$

The reciprocal lattice vector becomes $\boldsymbol{G} = n_1\boldsymbol{b}_1 + n_2\boldsymbol{b}_2 + n_3\boldsymbol{b}_3$ (where n_1, n_2, n_3 are integers). The zone boundaries of the first Brillouin zone in Fig. 1.1(b) are thus planes normal to $\pm(\pi/a)\boldsymbol{i}$, $\pm(\pi/a)\boldsymbol{j}$, $\pm(\pi/a)\boldsymbol{k}$, as shown in Figs. 1.1(b) and (c). The volume of the primitive reciprocal space is $\boldsymbol{b}_1 \cdot \boldsymbol{b}_2 \times \boldsymbol{b}_3 = (2\pi/a)^3$. The volume of the Fermi surface is $(2\pi/a)^3/2$ if one atom possesses one conduction electron, as in alkali metals of Li, Na, K, Rb, Cs and Fr.

Figure 1.3 shows the Fermi surfaces, based on the Harrison's free electron model, for the monovalent metal (Cu), divalent metal (Ca), trivalent metal (Al) and tetravalent metal (Pb) with the face-centered cubic structure [1]. The exact Fermi surfaces are slightly different from the Harrison's free electron model. For example, the neck Fermi surface exists along the $\langle 111 \rangle$ direction in Cu. The electron pocket Fermi surfaces in the fourth band of Pb do not exist. The first band of Pb is fully occupied by two of the electrons, and a closed Fermi surface in the second band is illustrated by the unoccupied (hole) Fermi surface, where another of its electrons occupies the second band. The last electron occupies the third band, revealing a "jungle gym" Fermi surface. In this case, the volume of the hole Fermi surface V_h in the second band is equal to the volume of the electron Fermi surface V_e in the third band. Pb is thus a compensated metal ($V_h = V_e$). On the other hand, Al is an uncompensated metal ($V_h \neq V_e$).

1.2 Crystal structure, crystal, and Fermi surface

For real metallic compounds, we will describe the framework of band theory. The usual band theory is based on the density functional formalism originating from the work of Hohenberg, Kohn and Sham [2, 3]. The wave function Ψ_i and the eigenvalue ε_i of an electron

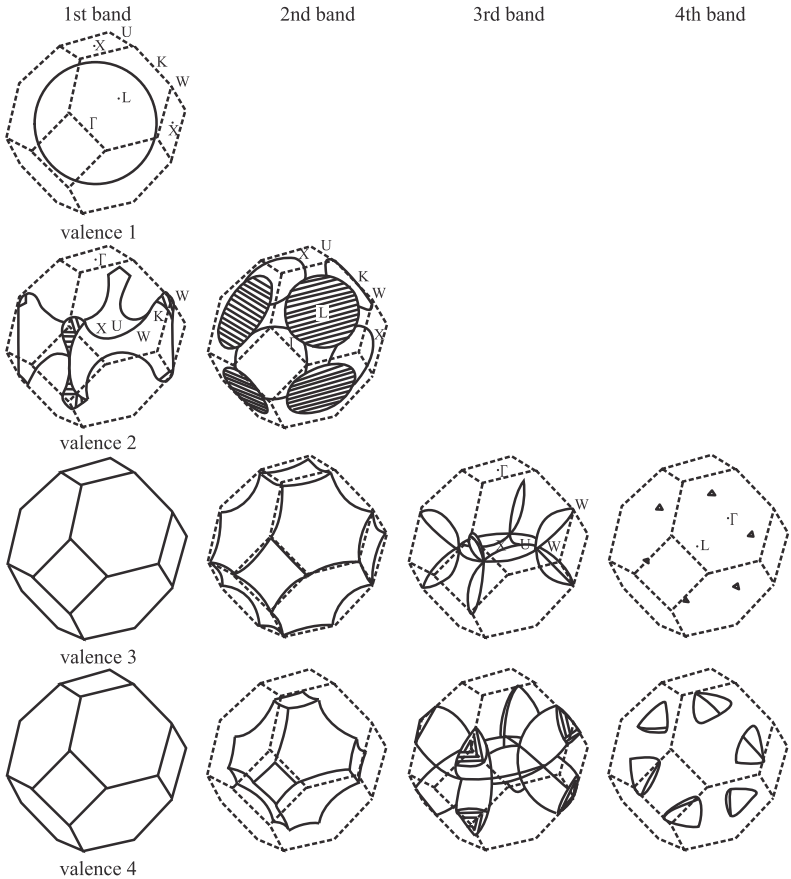

Figure 1.3: Fermi surfaces of Cu(valence 1), Ca(valence 2), Al(valence 3), and Pb(valence 4) with the face-centered cubic structure on the basis of the Harrison's free electron model, cited from Ref. [1].

in state i is given as a solution of the equation

$$\left\{-\frac{\hbar^2}{2m}\nabla^2 + U(\boldsymbol{r}) + e^2\int\frac{n(\boldsymbol{r}')}{|\boldsymbol{r}-\boldsymbol{r}'|}d\boldsymbol{r}' + v_{\rm xc}(\boldsymbol{r})\right\}\Psi_i(\boldsymbol{r}) = \varepsilon_i\Psi_i(\boldsymbol{r}) \tag{1.15}$$

where $n(\boldsymbol{r})$ is the electron density, given by

$$n(\boldsymbol{r}) = \sum_{i=1}^{N}|\Psi_i(\boldsymbol{r})|^2\,. \tag{1.16}$$

In the left-hand side of Eq. (1.15), the first term is the kinetic energy, the second term the nuclear potential, the third term a direct Coulomb potential, and the fourth term $v_{\rm xc}(\boldsymbol{r})$, the exchange-correlation potential defined by

$$v_{\rm xc}(\boldsymbol{r}) = \frac{\delta E_{\rm xc}[n]}{\delta n(\boldsymbol{r})} \tag{1.17}$$

where $E_{\rm xc}$ is the exchange-correlation energy, which should be a complicated functional of the electron density n. Its exact form is unknown. The most essential point is how a reasonably good and simple form of the functional for the exchange-correlation potential can be found. The local density functional or the local density approximation (LDA) proposed by Gunnarsson and Lundqvist [4] is a drastic approximation. This is based on the assumption that the electron density is a slowly varying function of space. The exchange-correlation potential is thus expressed as

$$v_{\rm xc}(\boldsymbol{r}) = \alpha e^2 \left[\frac{3}{\pi} n(\boldsymbol{r})\right]^{1/3} \tag{1.18}$$

where α is constant, for example $\alpha \simeq 0.7$.

In order to calculate the energy band structure of rare earth and uranium compounds, relativistic effects should be taken into account because the extremely strong nuclear potential extends into the core region of the atom. Note that lanthanides and actinides have high atomic numbers. In this case, the spin-orbit interaction is taken into account self-consistently for all the valence electrons as in a second variational procedure. Alternatively, we can use the Dirac one-electron wave function instead of Eq. (1.15). Some standard techniques to calculate the band structure self-consistently within a required accuracy are the Green's function or Korringa-Kohn-Rostoker (KKR) method, the linearized muffin-tin orbital (LMTO) method, and the augmented plane wave (APW) method or linearized APW (LAPW) method, etc [5].

Here, we show the exact Fermi surfaces. The topology of the Fermi surface changes as a function of the number of valence electrons. This is well known as the Harrison's free electron model mentioned above. A compensated metal ($V_e = V_h$) is extremely different from

an uncompensated metal ($V_e \neq V_h$) in topology. Here, V_e refers to the volume of an electron Fermi surface and V_h is the volume of a hole Fermi surface. For example, Fermi surface properties of rare-earth and actinide compounds with the $AuCu_3$-type cubic and $HoCoGa_5$-type tetragonal crystal structures have been shown to be functions of the number of valence electrons. See ref. [6] for details.

The dimensionality of the electronic state is another factor that changes the topology of the Fermi surface. If conduction electrons can move freely in real space, the topology of the Fermi surface is spherical, and this can be described as $\varepsilon_{\rm F} = (\hbar^2/2m^*)(k_x^2 + k_y^2 + k_z^2)$, as shown in Fig. 1.4(a). If conduction electrons can move only in the x-y plane and not along the z-axis, the topology of the Fermi surface changes from a sphere to a cylinder: $\varepsilon_{\rm F} = (\hbar^2/2m^*)(k_x^2+k_y^2)$, as shown in Fig. 1.4(b), revealing a two-dimensional electronic state. High-T_c cuprates are typical examples. If instead, the conduction electrons can move only along the z-axis [$\varepsilon_{\rm F} = (\hbar^2/2m^*)k_z^2$] the topology of the Fermi surface can be changed into two plates, as shown in Fig. 1.4(c). This is one-dimensional in the electronic state. In this case, the well-known Peierls instability is realized, and a one-dimensional conductor becomes an insulator. Organic conductors are typical examples.

When the electronic state at $\boldsymbol{k}$ is transferred by a propagation vector $\boldsymbol{q}$, the electronic or Fermi surface instability occurs at $\varepsilon_{\boldsymbol{k}} = \varepsilon_{\boldsymbol{k}+\boldsymbol{q}}$. Here, $\varepsilon_{\boldsymbol{k}}$ and $\varepsilon_{\boldsymbol{k}+\boldsymbol{q}}$ are the electronic energies at $\boldsymbol{k}$ and $\boldsymbol{k}+\boldsymbol{q}$, respectively. An overlapping region is, however, only one point for the spherical Fermi surface, as shown in Fig. 1.4(d), and one line along the k_z-axis for the cylindrical Fermi surface. In these cases, the Fermi surface instability is not realized. The overlapping of the Fermi surface for the propagation vector $\boldsymbol{q}$ is called "nesting". The nesting of the Fermi surface occurs for a characteristic two-dimensional compound, 1T-TaS_2, for example. Figure 1.4(e) shows the characteristic cylindrical Fermi surface in 1T-TaS_2 [7, 8]. The nesting is realized in a wide region of the Fermi surface. The overlapping region of the Fermi surface disappears in the two-(or three-)dimensional case of the Fermi surface instability, which is called "charge density wave" (CDW) instability. Correspondingly, the lattice is distorted with a

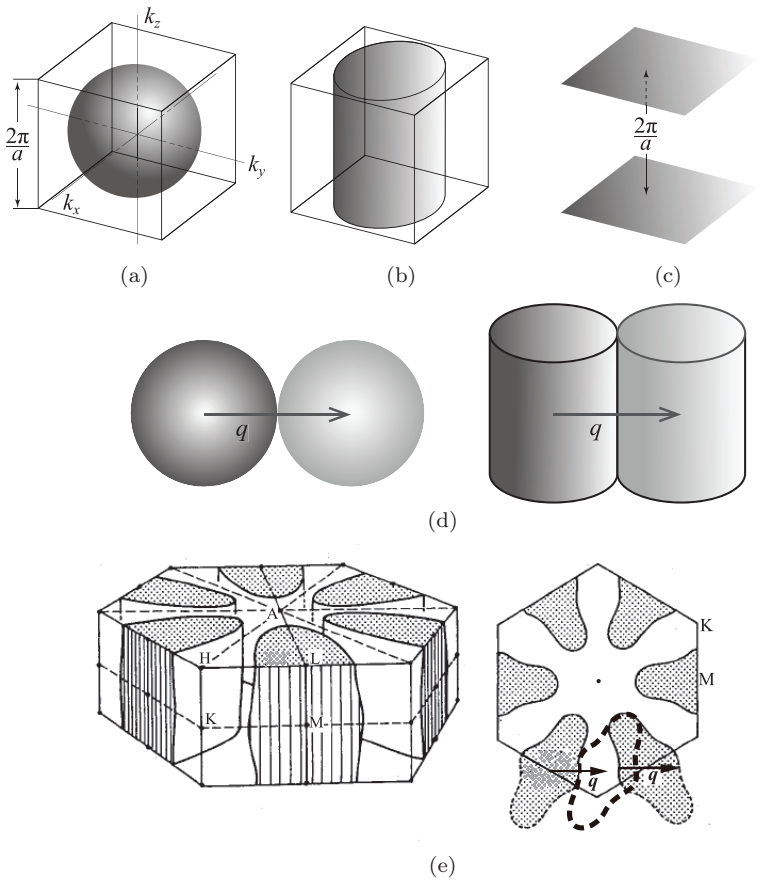

Figure 1.4: (a) Three-, (b) two-, and (c) one-dimensional Fermi surfaces, (d) nesting of the spherical and cylindrical Fermi surfaces, and (e) nesting of the Fermi surface in 1T-TaS_2, cited from Refs. [7, 8].

wavelength $2\pi/q$. A metallic state of 1T-TaS_2 at high temperatures with a carrier number of 10^{22} cm^{-3} is changed into an insulator at low temperatures with a carrier number of 10^{18} cm^{-3} (carriers of impurities), demonstrating an incommensurate CDW at 350 K with a partial disappearance of the Fermi surface, and a commensurate CDW at 180 K with a complete disappearance of the Fermi surface [9]. In this case, the term "commensurate" applies to the case where there is an integer number ratio of the reciprocal lattice vector $\boldsymbol{a}^*$ to the propagation vector $\boldsymbol{q}$, such as $3\boldsymbol{q} = \boldsymbol{a}^*$. A relation of

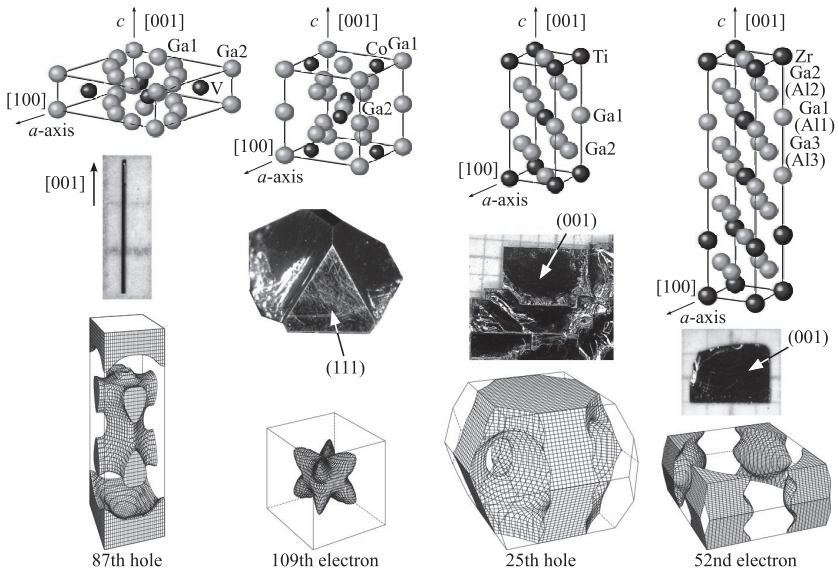

Figure 1.5: (From top to bottom) The tetragonal crystal structure, a single crystal, and corresponding Fermi surface in (a) V_2Ga_5, (b) $CoGa_3$, (c) $TiGa_3$, and (d) $ZrGa_3$ and $ZrAl_3$, cited from Ref. [10].

$3\boldsymbol{q}_1 - \boldsymbol{q}_2 = \boldsymbol{a}^*$ is realized in 1T-TaS_2, where $\boldsymbol{q}_i$ $(i = 1, 2, 3)$ is the propagation vector in the hexagonal lattice of 1T-TaS_2.

A change in Fermi surfaces based on the dimensionality of the electronic states can occur when the c/a ratio of the tetragonal structure is continuously changed. Figure 1.5 shows several different tetragonal structures in T-Ga (T: transition metal) binary compounds [10]. The following is a main point in this study: the smaller the tetragonal c-value, the more enhanced the one-dimensionality of the electronic state; the larger the c-value, the more enhanced the two-dimensionality. We expect that nearly one-dimensional characteristic Fermi surfaces can be realized in V_2Ga_5 (space group No. 127, $a = 8.936$ Å, $c = 2.683$ Å, formula units per cell $Z = 2$), and two-dimensional Fermi surfaces in $ZrGa_3$ (No. 139, $a = 3.965$ Å, $c = 17.461$ Å, $Z = 4$) and $ZrAl_3$. Fermi surfaces in $CoGa_3$ (No. 136, $a = 6.230$ Å, $c = 6.431$ Å, $Z = 4$) are three-dimensional

because the c-value is almost the same as the a-value. In contrast to these compounds, $TiGa_3$ (No. 139, $a = 3.789$ Å, $c = 8.734$ Å, $Z = 2$) crystallizes in a typical tetragonal structure as in $ThCr_2Si_2$.

Single crystals of these compounds have been grown by the Ga (Al) self-flux method, and de Haas-van Alphen (dHvA) experiments carried out, together with the full-potential linearized augmented plane wave (FLAPW) energy band calculations.

The characteristic shapes of single crystals in these compounds, as shown in Fig. 1.5, are interesting. The characteristic features of crystal structures and their corresponding single crystals are summarized below:

1) In V_2Ga_5, the crystal structure is flat along the tetragonal [001] direction (c-axis), and the corresponding single crystal is of needle shape along the [001] direction.
2) $CoGa_3$ is tetragonal in the crystal structure, but is approximately cubic, as shown in Fig. 1.5(b). Correspondingly, $CoGa_3$ is of pyramidal shape, which is characteristic of the crystals with the fcc structure, and also with the diamond-type structure. The flat plane of the pyramid corresponds to the (111) plane.
3) The shape of a single crystal in $TiGa_3$ is typically tetragonal. The flat plane of a rectangular single crystal corresponds to the tetragonal (001) plane (c-plane).
4) In $ZrGa_3$ and $ZrAl_3$, the crystal structure is elongated along the tetragonal [001] direction, and the corresponding single crystal is of thin-plate shape, of which the flat plane corresponds to the tetragonal (001) plane.

Reflecting the crystal structures or the corresponding Brillouin zones, the Fermi surfaces have characteristic properties which have been clarified through dHvA experiments and energy band calculations. They are summarized as follows:

1) A nearly one-dimensional plate-like Fermi surface is obtained in the band calculation, as shown in Fig. 1.5(a). The plate is, however, wavy in shape, and the electronic state is not

Table 1.1: Electronic specific heat coefficients γ in V_2Ga_5, $CoGa_3$, $TiGa_3$, $ZrGa_3$, and $ZrAl_3$ and the corresponding theoretical values γ_b, cited from Ref. [10].

	γ mJ/(K^2·mol)	γ_b mJ/(K^2·mol)	γ/γ_b
V_2Ga_5	16.7	10.41	1.60
$CoGa_3$	2.5	2.32	1.08
$TiGa_3$	3.6	3.57	1.01
$ZrGa_3$	2.5	2.41	1.04
$ZrAl_3$	2.7	2.50	1.08

one-dimensional but nearly three-dimensional. Therefore, Peierls instability is not realized in this compound.

2) The Fermi surfaces in $CoGa_3$ are very similar to those of Ni_3Ga with the $AuCu_3$-type cubic structure. The band 109th electron Fermi surface is typical between the two compounds, as shown in Fig. 1.5(b).
3) The Fermi surfaces in $TiGa_3$ are also very similar to those of YCu_2Si_2 with the $ThCr_2Si_2$-type tetragonal structure. The band 25th hole Fermi surface is typical between the two compounds, as shown in Fig. 1.5(c).
4) The flat Brillouin zone often produces the cylindrical Fermi surface, which is realized in $ZrGa_3$ and $ZrAl_3$. The band 52nd electron Fermi surface is typical, possessing concave and convex shapes in the cylinder.

Finally, we summarize in Table 1.1 the γ values of these compounds and the corresponding theoretical γ_b values. The γ value of 16.7 mJ/(K^2·mol) of V_2Ga_5 is slightly larger than γ_b of 10.41 mJ/(K^2·mol), which is characteristic in the 3*d*-electron system. The experimental and theoretical values of the others compounds are approximately the same under consideration of a small mass enhancement based on the electron–phonon interaction.

1.3 Interacting conduction electrons -Fermi liquid-

The concept of the Fermi surface has already been introduced earlier in the one-electron band theory of metals in which the

electron-electron interactions (correlations) are treated to some extent. It is important to check experimentally the magnitude of the electron-electron interaction in metals. This was obtained by measuring the electrical resistivity below 1.5 K, for example, for Al [11]. The resistivity ρ is expressed as

$$\rho = \rho_0 + AT^2.$$

The term $AT^2 (= \rho_{e\text{-}e})$ is due to the electron-electron scattering. The corresponding two electrons are occupied within a small energy region of $k_{\rm B}T$ from the Fermi energy $\varepsilon_{\rm F}$. This is because the initial states of two scattering electrons are occupied in a Fermi surface while the final states after the electron-electron scattering correspond to two unoccupied states by the Pauli principle. The AT^2 term is simply obtained from a relation of $\rho_{e\text{-}e} \sim \tau^{-1} \sim (k_{\rm B}T/\varepsilon_{\rm F})^2 \sim T^2$, where $\varepsilon_{\rm F} \sim m^{*\,-1}$ from Eq. (1.8b) and τ is the scattering lifetime. Note that the mass of Eq. (1.8b) is m. This is changed to the effective mass m^*, considering the mass enhancement of the electron-electron interaction. The low-temperature (below 1.5 K) electrical resistivity is of the form $\rho = \rho_0 + AT^2$ ($A = 3 \times 10^{-7}$ $\mu\Omega$·cm/K^2) in Al. This is very small in value. Experimentally, it is very difficult to detect the electron-electron interaction in the usual metal. In the heavy fermions of some rare earth and uranium compounds, the AT^2 term is extremely large and not negligible — for example, $A = 10^2$ $\mu\Omega$·cm/K^2 in $YbCo_2Zn_{20}$, which is shown later. Note that $\sqrt{A}$ is proportional to m^*, or $A \propto m^{*2}$.

Landau investigated the interacting fermion system of ^{3}He. The theoretical results are known as Landau's Fermi liquid theory, which are applied to interacting electrons in metals [12]. Landau arrived at a surprising conclusion. A system of interacting electrons can be attained when we start from a system of non-interacting electrons and slowly turn on the interaction. The ground state and low-lying excitations of Fermi liquid are therefore in one-to-one correspondence to those of the non-interacting Fermi gas. Note that the distribution function in the ground state for the interacting electrons $n(\boldsymbol{k}\sigma)$ is changed, shown schematically in Fig. 1.6(a), which is compared with the usual Fermi-Dirac distribution function of $n(\boldsymbol{k}) = 1/[(\varepsilon_{\boldsymbol{k}} - \mu)/k_{\rm B}T + 1]$ in Fig. 1.6(b). Here, μ is the chemical

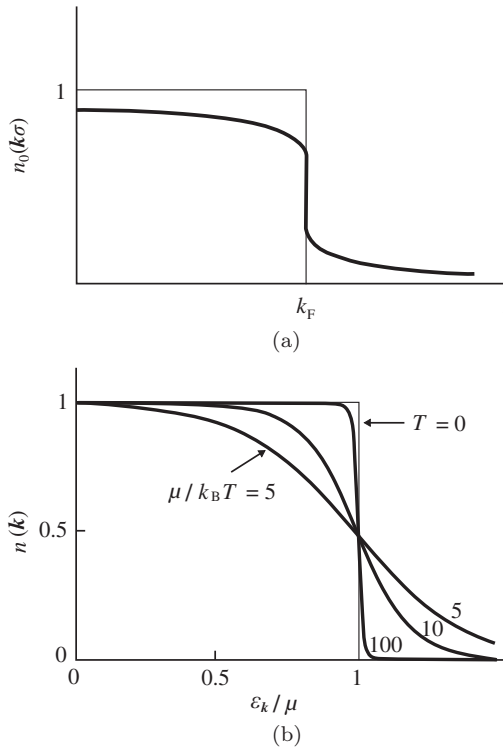

Figure 1.6: (a) Distribution function in the ground state for interacting electrons and (b) the Fermi-Dirac distribution function as a function of temperature.

potential. However, a sharp step at k_F remains from the one-to-one correspondence mentioned above. A change in the energy δE caused by a change in the distribution function of $n(\boldsymbol{k}\sigma) = \boldsymbol{n_0}(\boldsymbol{k}\sigma) + \delta n(\boldsymbol{k}\sigma)$ is given by

$$\delta E = \sum_{\boldsymbol{k}} \sum_{\sigma} \varepsilon_{\boldsymbol{k}} \delta n(\boldsymbol{k}\sigma) + \frac{1}{2} \sum_{\boldsymbol{k}} \sum_{\sigma} \sum_{\boldsymbol{k}'} \sum_{\sigma'} \times f(\boldsymbol{k}, \sigma, \boldsymbol{k}', \sigma') \delta n(\boldsymbol{k}, \sigma) \delta n(\boldsymbol{k}', \sigma') \tag{1.19}$$

where the function $f(\boldsymbol{k}, \sigma, \boldsymbol{k'}, \sigma')$, which was introduced by Landau, is unknown, but characterizes the electron-electron interaction. The theoretical results obtained from Landau's Fermi-liquid theory are as follows. The effective mass m^* of the interacting electrons is

enhanced as

$$m^* = m\left(1 + \frac{F_1^s}{3}\right). \tag{1.20}$$

The interacting electrons are called "quasiparticles" in Landau's Fermi-liquid theory, where names correspond to "dressed electrons". F_1^s is the interaction parameter derived from $f(\boldsymbol{k}, \sigma, \boldsymbol{k}', \sigma')$, together with F_0^a shown later. The electronic specific heat coefficient γ is given as

$$\gamma = \frac{2\pi^2 k_{\mathrm{B}}^2}{3} D^*(\varepsilon_{\mathrm{F}}). \tag{1.21}$$

The spin susceptibility χ_s is

$$\chi_s = \frac{2\mu_{\mathrm{B}}^2 D^*(\varepsilon_{\mathrm{F}})}{1 + F_0^a}. \tag{1.22}$$

The factor $1/(1 + F_0^a)$ corresponds to the Stoner enhancement factor shown in Chap. 4.

The effective mass m_c^* determined by the de Haas-van Alphen experiment is usually different from the band mass m_b, particularly in Ce, Yb, and U compounds. Here, the experimental γ and m_c^* values are usually larger than the theoretical γ_b and m_b values, which are obtained by the energy band calculations. The mass enhancement factor λ is defined as:

$$\frac{\gamma}{\gamma_b} = \frac{m_c^*}{m_b} = 1 + \lambda.$$

Origins for λ are ascribed to the many-body effects, which cannot be taken into account in the usual band theory. As for most probable origins, the electron-phonon interaction and the magnetic interactions are considered, and their contributions are denoted by λ_p and λ_m, respectively. Therefore, λ is expressed as a sum of two contributions

$$\lambda = \lambda_p + \lambda_m.$$

The electron-phonon term λ_p in normal metals such as Pb, including its temperature dependence, is well understood at present. Its magnitude is smaller that 1. If it were large, it might cause lattice instability. In contrast to this small value of λ_p, the magnetic

contribution λ_m can take a large value in some Ce, Yb, and U compounds.

The magnetic contribution λ_m can be divided into two cases according to its origins. The first case occurs in many lanthanide compounds in which the $4f$ electrons are localized at lanthanide ions and their spin fluctuations enhance the effective mass of the conduction electrons via c–f interactions such as the Ruderman-Kittel-Kasuya-Yosida (RKKY) interaction, where c stands for conduction electrons and f for $4f$ electrons. A small mass enhancement of $\lambda_m = 1{-}2$ is observed in lanthanide compounds.

Another magnetic contribution to λ_m occurs when the $3d$ electrons in the ion-series transition metal compounds are itinerant and their spins are fluctuating. The magnitude of λ_m is, however, not extremely large; $\lambda_m = 1{-}5$ in the $3d$ electron system. In some Ce, Yb, and U compounds, λ_m is extremely large; $\lambda_m = 60$ in $CeRu_2Si_2$, for example, which is described later. The f electrons in these Ce, Yb, and U compounds are localized at temperatures higher than room temperature, but become itinerant at low temperatures, via the Kondo effect. The heavy f-electron system is a main theme in this text.